



Feasibility study of a desiccant packed bed system for air humidification

Stefano De Antonellis^a, Luigi Colombo^a, Angelo Freni^{b,*}, Cesare Joppolo^a

^a Politecnico di Milano, Dipartimento di Energia, Via Lambruschini 4, 20156, Milan, Italy

^b CNR ICCOM, Institute of Chemistry of Organometallic Compounds, Via G. Moruzzi 1, 56124, Pisa, Italy



ARTICLE INFO

Article history:

Received 27 May 2020

Received in revised form

31 July 2020

Accepted 2 October 2020

Available online 7 October 2020

Keywords:

Desiccant

Packed bed

Humidification

Silica gel

ABSTRACT

In winter conditions air humidifiers are particularly important because low indoor relative humidity can lead to occupants' discomfort, such as dry throat, skin and eyes and, in addition, it can facilitate virus and bacteria transmission among persons. In this work, a study of a novel humidification system based on silica gel packed beds is carried out. In the proposed device, vapour is adsorbed from the exhaust airflow leaving the building and it is released to the fresh air stream supplied to the indoor environment. The analysis is carried out through both experimental and numerical approach: a specific test rig has been implemented to evaluate performance of the packed bed apparatus and obtained data have been used to validate a phenomenological model. The adsorption isotherm and the heat of adsorption of the adopted silica gel have been evaluated through a gravimetric approach. Numerical results highlight the proposed system can provide satisfactory air humidification even when it is driven by low temperature heat sources. Depending on bed thickness, airflows arrangement and air velocity, the humidity ratio of airflow supplied to the building can be increased from 1.5 g kg^{-1} to $4.8\text{--}5.8 \text{ g kg}^{-1}$ when the indoor humidity ratio is 5.8 g kg^{-1} and the regeneration temperature is around $50 \text{ }^\circ\text{C}$.

© 2020 Elsevier Ltd. All rights reserved.

1. Introduction

In cold climates, low relative humidity in indoor environments is related to occupants' discomfort and health issues [1,2]. In particular, low relative humidity can lead to dry nose, throat and eyes, headache and skin irritation. In addition, it can facilitate virus and bacteria transmission among people [3]. At present, recommended minimum relative humidity values [4] are around 30–40% for most built environments, such as offices, homes, schools and hospitals. For this reason, there is a significant interest in the design, optimization and management of air humidifiers, which can provide the adequate quantity of water vapour to the indoor air in order to reach the desired relative humidity.

Commercial humidifiers can be classified in two main groups: adiabatic systems and isothermal systems [4]. In the first case, air is humidified through liquid water: a quasi-isenthalpic process occurs, with an increase in the humidity ratio and a decrease in the dry bulb temperature. Moist air provides the evaporation enthalpy to liquid water, hence it cools down. In the second case,

humidification is achieved directly providing steam, which is generated in an appropriate device, to the air stream. The process is almost isothermal: the moist air undergoes an increase in humidity ratio with a contextual slight increase in the dry bulb temperature. Due to the low cost and the low temperature heat source required to promote water evaporation, adiabatic humidifiers are particularly adopted in conventional applications. Anyway, the main issue of these systems is the risk of bacterial proliferation related to the presence of water droplets. For this reason, in some applications (e.g. hospitals) isothermal humidifiers are preferred, since the small steam molecules limit bacteria growth and the high steam temperature kills most of pathogens. However, steam humidifiers are driven by electricity or high temperature heat sources, with consequent high primary energy consumption.

At present, there is an increasing interest in innovative humidification systems that can limit the aforementioned technical and health issues. In particular, research efforts deal with the use of sorption materials to transfer water vapour between two air streams: in this way, through an appropriate arrangement of the components, the airflow supplied to the building can be effectively humidified. In these systems there is not liquid water, with consequent minimal risks of air contamination, and the sorption

* Corresponding author.

E-mail address: angelo.freni@pi.iccom.cnr.it (A. Freni).

| Nomenclature | | | |
|----------------------|---|---------------------|--|
| A | Adsorption potential (J kg^{-1}) | ρ | Density (kg m^{-3}) |
| cp | Specific heat capacity at constant pressure ($\text{J kg}^{-1} \text{ } ^\circ\text{C}^{-1}$) | τ | Commutation time - half cycle (s) |
| D | Diameter (m) | <i>Superscripts</i> | |
| E | Characteristic Dubinin-Astakhov parameter (J kg^{-1}) | N | Reference condition ($\rho = 1.2 \text{ kg m}^{-3}$) |
| h | Specific enthalpy (J kg^{-1}) | <i>Subscripts</i> | |
| H | Height (m) | a | Dry air |
| h_a | Specific dry air enthalpy (J kg^{-1}) | cv | Control volume |
| h_c | Heat transfer coefficient ($\text{W m}^{-2} \text{ } ^\circ\text{C}^{-1}$) | ads | Adsorption material |
| h_m | Mass transfer coefficient ($\text{kg m}^{-2} \text{ s}^{-1}$) | b | Desiccant bead |
| h_v | Specific water vapour enthalpy (J kg^{-1}) | bed | Desiccant bed |
| n | exponent for surface heterogeneity (–) | el | Electrical |
| p | Pressure (Pa) | f | Face |
| q | Specific energy consumption (J kg^{-1}) | ht | High temperature |
| Q_{ads} | Heat of adsorption (J kg^{-1}) | in | Inlet |
| Re | Reynolds number (–) | lt | Low temperature |
| RH | Relative humidity (–) | max | Maximum |
| S | Surface area (m^2) | out | Outlet |
| t | Time (s) | p | Primary energy source |
| T | Dry bulb temperature ($^\circ\text{C}$) | pro | Process air stream |
| \bar{T} | Average dry bulb temperature ($^\circ\text{C}$) | reg | Regeneration air stream |
| v | Velocity (m s^{-1}) | sat | Saturation condition |
| V | Volume (m^3) | t | Time |
| W | Water content (kg kg^{-1}) | th | Thermal |
| x | Flow direction (m) | tot | Total |
| X | Humidity ratio (kg kg^{-1}) | v | Water vapour |
| \bar{X} | Average humidity ratio (kg kg^{-1}) | w | Water |
| <i>Greek letters</i> | | <i>Acronyms</i> | |
| Δ | Variation | AH | Adiabatic Humidifier |
| ε | Void fraction (–) | AHU | Air Handling Unit |
| η | Efficiency (–) | DH | Desiccant Humidifier |
| λ | Heat of evaporation of water (J kg^{-1}) | EXP | Experimental |
| ν | Kinematic viscosity ($\text{m}^2 \text{ s}^{-1}$) | NUM | Numerical |
| | | SH | Steam Humidifier |

material can be regenerated at low temperature (around 40–50 °C), with resulting primary energy savings and possible integration with renewable energy sources. In particular, this technology can be coupled with solar thermal collectors, cogenerators or driven by industrial waste heat or district heating. Finally, these systems can even have a sanitizing effect on airborne microorganisms [5,6].

Desiccant materials are already widely adopted in enthalpy wheels for passive water vapour recovery between exhaust and fresh airflows. Recent studies focus on the experimental and numerical analysis of rotary heat exchanger performance, showing that latent effectiveness can reach 75% in normal operating conditions [7] or 89% in high temperature difference condition [8], and on its integration in actual air conditioning systems [9], highlighting its energetic benefits on yearly basis. Instead, the use of sorption materials for active air humidification is an emerging technology: at present main research efforts deal with the use of desiccant wheels, packed beds or coated heat exchangers. La et al. [10] and Zeng et al. [11] analysed a one-rotor two-stage desiccant wheel systems for air heating and humidification coupled with solar collectors. Moisture is removed from exhaust air stream and supplied to the fresh one. It is shown the system can improve occupants' comfort due to the increase in indoor humidity compared to conventional configurations. In particular, La et al. [10] showed the time within comfort zone is increased from around 10%–20%

for the standalone solar heating system. Instead, Zeng et al. [11] showed that in the optimized system around 60% of the airflow humidification can be managed through the desiccant system. Similarly, Kawamoto et al. [12] carried out an experimental analysis of an actual air conditioning system providing air humidification through a desiccant wheel. The research highlights the humidity ratio of outdoor air can be increased from 1.8 - 2.3 g kg^{-1} to 5.8 g kg^{-1} before being supplied to the building. De Antonellis et al. [13] and Cazzaniga et al. [14] investigated two systems for hospital applications in which water vapour is transferred between two airflows at outdoor conditions: the first one is dehumidified and used as vapour source while the second one is humidified and supplied to the building. In the first research [13] the sorption apparatus is a desiccant wheel while in the second one [14] it consists of two desiccant packed beds. Results put in evidence that in typical Southern Europe winter outdoor conditions, the system can provide adequate air humidification: process to regeneration mass flow ratio higher than 1.3 is suggested in the first work [13] and around 1.5 in the second one [14]. Recently, Tu et al. [15] carried out a numerical analysis to optimize sorption humidification systems, recommending configurations with three stages of desiccant wheels. In addition, a few patents deal with sorption based humidification system. Inventions concern different systems that can selectively switch between dehumidification and humidification

operation [16,17] or between conventional water vapour recovery and active air humidification [18]. Finally, some studies focus on the use of fin and tube desiccant coated heat exchanger for air humidification. This configuration is of particular interest because heat for regeneration can be provided continuously to the airflow, reducing the source temperature. Sun et al. [19] investigated the influence of different structures and desiccant materials on the humidification capacity, indicating that the potassium-based compound performs better than others. Ge et al. [20] and Zhang et al. [21] performed numerical simulations to evaluate performance in winter conditions, suggesting respectively a regeneration temperature around 30 °C and 40 °C. Finally, Valarezo et al. [22] carried out an experimental investigation focused on novel desiccant compounds, evaluating that a silica gel and sodium coating is optimal in winter condition.

Available scientific and technical literature highlights that the use of desiccant materials for air humidification has great potential and many possible applications. Anyway, many efforts should be still done to overcome existing gaps, in particular evaluating optimal system design, configuration and manufacturing process, most appropriate sorption materials and effective control logic.

The scope of this research is to perform a feasibility study about the use of silica gel packed beds for air humidification. In the investigated system, water vapour is extracted from the exhaust airflow leaving the building, which is characterized by a higher humidity ratio than outdoor air. In this configuration, it is possible to realize a simple and compact device that can actively transfer a higher amount of water vapour than conventional passive sorption recovery systems, such as enthalpy wheels. In addition, packed beds can be easily manufactured and integrated with commercial devices for airflow commutation [23] and silica gel beads are widely available and cheap.

Main novelties of the proposed study are: i) the detailed performance analysis of the silica gel packed bed humidifier operating between fresh and exhaust airflows; ii) the evaluation of optimal system design at low regeneration temperature; iii) an energy consumption comparison among desiccant and conventional humidifiers.

The research is carried out through a comprehensive approach, integrating the experimental analysis of the humidifier in a dedicated test rig, the characterization of sorption properties of the adopted desiccant material and the development of a phenomenological model of a packed bed system. Results of this work provide a guidance to the design of the humidification system and can be effectively used by engineers operating in the HVAC industry.

2. System description and methodology

The proposed system consists of two packed beds, filled with desiccant beads, which are alternatively crossed by two airflows, namely the process and regeneration ones. According to the conventional terminology adopted in literature for air desiccant dehumidification, the process air stream is heated and dehumidified and the regeneration one is cooled and humidified. In order to effectively remove water vapour from the desiccant material, the regeneration airflow is adequately heated before entering the bed. According to the scheme of Fig. 1, in the proposed system:

1. The process airflow (blue line) is the return one from the building. It is at indoor air conditions and it is dehumidified through the desiccant bed. At the end of the process it is discharged to the surrounding environment.
2. The regeneration airflow (red line) is the fresh one supplied to the indoor environment. It is at outdoor air conditions and it is

humidified crossing the bed. At the end of the process it is supplied to the indoor environment.

Therefore, the humidification of the regeneration airflow occurs thanks to the removal of water vapour from the return stream.

The research is carried out through the following steps:

1. A phenomenological model of the packed bed system is implemented.
2. Adsorption isotherm and heat of adsorption of adopted silica gel are experimentally evaluated.
3. A dedicated setup to test desiccant packed bed systems is realized and experiments are carried out.
4. Experimental data and numerical results are compared in order to validate the model.
5. A comprehensive parametric analysis is carried out to evaluate system performance in different operating conditions and configurations.
6. Specific energy consumption of the system is compared to ones of conventional technologies.

Performance of the proposed humidification system are mainly evaluated through the average outlet humidity ratio $\bar{X}_{a,out}$ and air temperature $\bar{T}_{a,out}$ of both airflows, calculated in the following way:

$$\bar{X}_{a,out} = \frac{\int_{t=0}^{\tau} X_{a,out} dt}{\tau} \quad (1)$$

$$\bar{T}_{a,out} = \frac{\int_{t=0}^{\tau} T_{a,out} dt}{\tau} \quad (2)$$

Where τ is the duration of the commutation period (half cycle) and the subscript a refers to the process or regeneration airflow.

In addition, performance is evaluated in terms of average humidity ratio and temperature variation of the two air streams:

$$\Delta \bar{X}_a = \bar{X}_{a,out} - \bar{X}_{a,in} \quad (3)$$

$$\Delta \bar{T}_a = \bar{T}_{a,out} - \bar{T}_{a,in} \quad (4)$$

Where average inlet conditions are evaluated by the same methodology reported in Eqs. (1) and (2).

3. Modelling of the system

3.1. Model description

The numerical analysis of this research is carried out through a phenomenological model of the desiccant packed bed system. The model is based on the previous research of Pesaran and Mills [24] regarding the study of silica gel packed beds. In order to limit the computational time, a simplified approach, based on cross-section area averaging has been adopted [25]. Actually, owing to the boundary conditions and in the absence of flow maldistribution, the dependence of water content and temperature is reasonably weaker upon directions normal to the bulk flow than along it. Accordingly, the local values of water content and temperature can be replaced with their cross-section averages and an infinitesimal control volume is taken as shown in Fig. 2. The main assumptions of the simplified model are:

- Uniform air inlet conditions.

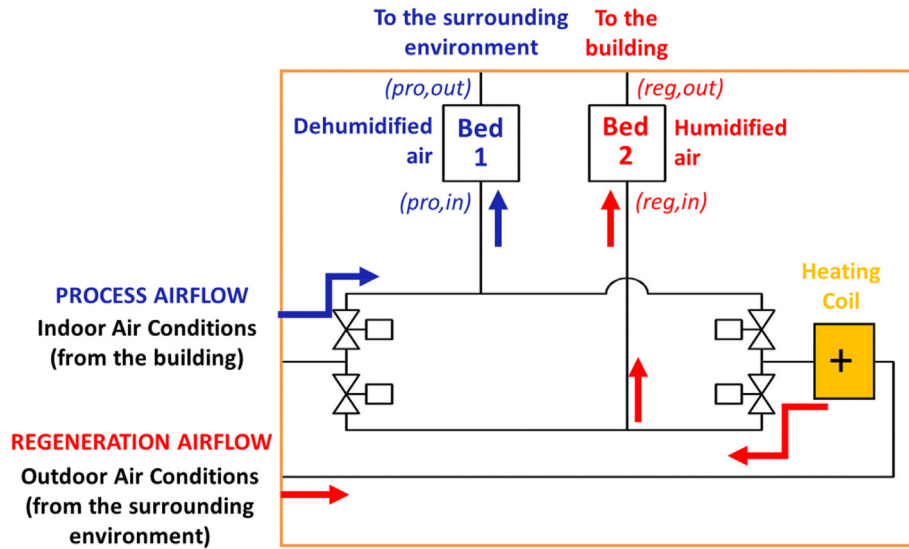


Fig. 1. Working principle of the proposed humidification system.

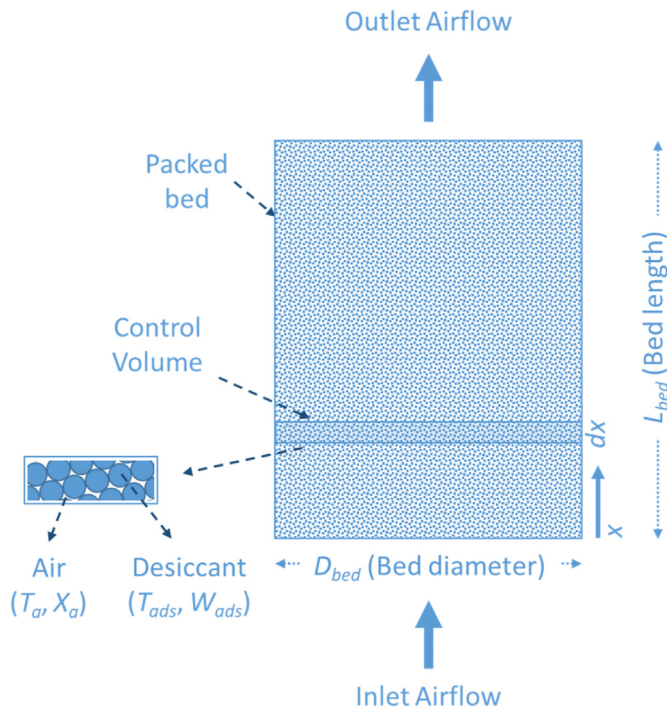


Fig. 2. Scheme of the desiccant beads packed bed.

- One dimensional air flow (x direction).
- Negligible axial heat conduction and water vapour diffusion in the air stream and in the desiccant bed.
- No heat losses to the surrounding.
- Uniform temperature and water content within desiccant particles.
- No hysteresis effects in the desiccant material.
- Constant total pressure ($p_{tot} = 101325$ Pa).

The equations applied to the infinitesimal control volume of the bed (specific quantities are referred to dry air mass) are reported in the following.

Dry air mass balance in the air stream:

$$\frac{\partial M_a}{\partial t} = -S_{f,cv} \frac{\partial (v_a \rho_a)}{\partial x} \quad (5)$$

Water mass balance in the air stream:

$$\frac{\partial (M_a X_a)}{\partial t} = -S_{f,cv} \frac{\partial (v_a \rho_a X_a)}{\partial x} - S_{b,cv} h_m (X_a - X_{ads}) \quad (6)$$

Energy balance in the air stream:

$$\begin{aligned} \frac{\partial (M_a h_a)}{\partial t} = & -S_{f,cv} \frac{\partial (v_a \rho_a h_a)}{\partial x} - S_{b,cv} h_c (T_a - T_{ads}) \\ & - S_{b,cv} h_m h_v (X_a - X_{ads}) \end{aligned} \quad (7)$$

Water mass balance in the desiccant beads:

$$\frac{d(M_{ads} W_{ads})}{dt} = S_{b,cv} h_m (X_a - X_{ads}) \quad (8)$$

Energy balance in the desiccant beads:

$$\begin{aligned} \frac{d(M_{ads} h_{ads} + M_{ads} W_{ads} h_{w,ads})}{dt} = & S_{b,cv} h_c (T_a - T_{ads}) \\ & + S_{b,cv} h_m h_v (X_a - X_{ads}) \end{aligned} \quad (9)$$

Where area and volume quantities are evaluated as:

$$S_{f,cv} = \pi \left(\frac{D_{bed}}{2} \right)^2 \quad (10)$$

$$V_{tot,cv} = S_{f,cv} dx \quad (11)$$

$$S_b = 4\pi \left(\frac{D_b}{2} \right)^2 \quad (12)$$

$$V_b = \frac{4}{3} \pi \left(\frac{D_b}{2} \right)^3 \quad (13)$$

$$\varepsilon = \frac{V_{a,cv}}{V_{tot,cv}} \quad (14)$$

$$S_{b,cv} = \frac{V_{ads,cv} S_b}{V_b} = \frac{(1-\varepsilon)V_{tot,cv}}{\frac{4}{3}\pi\left(\frac{D_b}{2}\right)^3} 4\pi\left(\frac{D_b}{2}\right)^2 = \frac{3(1-\varepsilon)V_{tot,cv}}{\left(\frac{D_b}{2}\right)} \quad (15)$$

$$= \frac{3(1-\varepsilon)S_{f,cv} dx}{\left(\frac{D_b}{2}\right)}$$

The adopted correlations of heat and mass transfer coefficients, including the effect of water mass diffusion and heat conduction through desiccant beads, are those proposed by Pesaran and Mills [24]:

$$h_c = 0.683cp_a\nu_a\rho_a Re^{-0.51} \quad (16)$$

$$h_m = 0.704\nu_a\rho_a Re^{-0.51} \quad (17)$$

Where Reynolds number Re and face velocity ν_a are calculated in this way:

$$Re = \frac{\nu_a D_b}{\nu} \quad (18)$$

$$\nu_a = \frac{\dot{V}_a}{\pi\left(\frac{D_{bed}}{2}\right)^2} \quad (19)$$

The adsorption equilibrium relation is assumed dependent on temperature and relative humidity, without hysteresis effects. In the present work, W_{ads} , RH and T are related through the Dubinin-Astakhov equation [26] in the following form:

$$W_{ads} = W_{ads,max} e^{-\left(\frac{A}{E}\right)^n} = W_{ads,max} e^{-\left(\frac{RT_{ads} \ln(1/RH_{ads})}{E}\right)^n} \quad (20)$$

Where A is the adsorption potential, $W_{ads,max}$ is the maximum sorption capacity, E is the characteristic Dubinin-Astakhov parameter and n is an exponent that describes the surface heterogeneity.

The humidity ratio on the desiccant surface X_{ads} is calculated from conditions T_{ads} and RH_{ads} in this way:

$$X_{ads} = 0.622 \frac{P_{v,sat}(T_{ads})RH_{ads}}{P_{tot} - P_{v,sat}(T_{ads})RH_{ads}} \quad (21)$$

Finally, the heat of adsorption $Q_{ads} = h_v - h_{w,ads}$ is calculated through Clausius-Clapeyron equation [26]:

$$Q_{ads} = \lambda \frac{\partial \ln p_v}{\partial \ln p_{v,sat}} \Big|_{W_{ads}} \quad (22)$$

Where λ is the latent heat of evaporation of water at a given temperature. The terms $W_{ads,max}$, E and n used in this research have been estimated for the adopted desiccant material through a gravimetric approach, as discussed in detail in next Section 3.2.

The set of governing equations is alternatively solved for the process and regeneration airflow thorough appropriate variation of boundary conditions. It is assumed the same duration of process and regeneration period ($\tau_{pro} = \tau_{reg} = \tau$). The PDE system has been discretized through the Euler implicit method: a time step of 1 s and a space step of 0.5 cm have been adopted in most simulations. In addition, code runs have been repeated for several total cycle (process and regeneration) until results were independent of the initial conditions.

3.2. Sorption material characterization

3.2.1. Preliminary considerations and adopted methodology

The desiccant material adopted in the packed bed system is micro-porous silica gel SIOGEL® by Oker-Chemie GmbH. The material is in the form of spherical beads with average particle diameter D_b equal to 3.3 mm. Selected properties of the silica gel are reported in Table 1.

Water adsorption isotherms have been measured at 30 °C, 50 °C and 70 °C through a gravimetric adsorption apparatus (Aquadyne DVS). The anhydrous reference state was obtained in nitrogen atmosphere at 80 °C. Experimental uncertainty of temperature, relative humidity and mass of the gravimetric apparatus are respectively: ± 0.2 °C; from $\pm 0.8\%$ at 20 °C to $\pm 1.8\%$ at 70 °C; 1.0 μg plus 0.001% of suspended mass.

3.2.2. Adsorption equilibrium isotherm and reference density

Experimental data have been used to fit parameters of Eq. (20): obtained parameters are $W_{ads,max} = 0.3185$ kg kg⁻¹, $E = 202.3$ kJ kg⁻¹ and $n = 1.557$. Measured adsorption equilibrium isotherms at 30 °C, 50 °C and 70 °C and numerical results are reported in Fig. 3, as a function of relative humidity and of the adsorption potential. Obtained values are in agreement with ones of similar regular density silica gel reported in literature [25,27,28].

Finally, the reference density of silica gel beads was estimated through a gravimetric approach. Around one hundred grams of material have been dried for several days at 80 °C in nitrogen atmosphere until no weight variation was observed. In this way, the material reached the same condition adopted as reference state in the equilibrium water adsorption analysis previously discussed. Then, silica gel beads have been introduced in a cylindrical container (with both vessel height and diameter 15 times higher than average desiccant particles diameter) in order to fill it, as it occurs in the actual packed bed. The density of the packed bed $\rho_{ads,bed}$ (ratio between measured silica gel mass and inner cylinder volume) was equal to 844 kg m⁻³. The density of desiccant beads ρ_{ads} has been evaluated assuming perfectly spherical particles with uniform diameter. Consequently, a void ratio ε equal to 0.372 was considered, resulting $\rho_{ads} = \rho_{ads,bed}/(1-\varepsilon) = 1344$ kg m⁻³.

3.2.3. Heat of adsorption

The heat of adsorption has been calculated according to Eq. (22). Anyway, considering that the Dubinin-Astakhov approach has been used to correlate water content, temperature and relative humidity of the adopted desiccant material at equilibrium, the heat of adsorption can be simply calculated as $Q_{ads} = \lambda + A$ [29]. Obtained values are in agreement with data available in literature, such as ones measured by Goldsworthy [27] or summarized by Frazzica and Cabeza [29]: at low water content Q_{ads}/λ is around 1.2 while, at maximum sorption capacity, it approaches 1. Calculated trends of Q_{ads} at three different temperatures are shown in Fig. 4.

Table 1
Properties of adopted silica gel.

| | |
|---|----------|
| Average particle size [mm] | 3.3 |
| Surface Area [m ² g ⁻¹] | 800 |
| Pore volume [cm ³ g ⁻¹] | 0.4 |
| Average pore diameter [nm] | 2 |
| Specific Heat [kJ Kg ⁻¹ K ⁻¹] | 0.92 |
| Thermal conductivity [W m ⁻¹ K ⁻¹] | 0.14–0.2 |

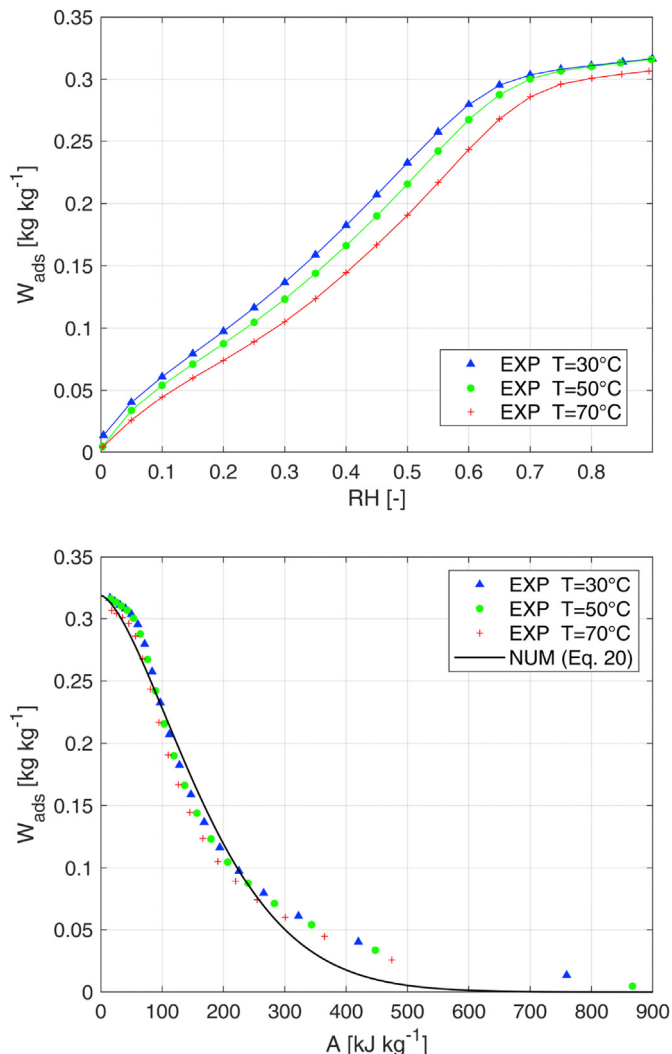


Fig. 3. Measured and calculated equilibrium adsorption capacity of silica gel (numerical results obtained with Eq. (20) and the following parameters: $W_{ads,max} = 0.3185 \text{ kg kg}^{-1}$, $E = 202.3 \text{ kJ kg}^{-1}$ and $n = 1.557$).

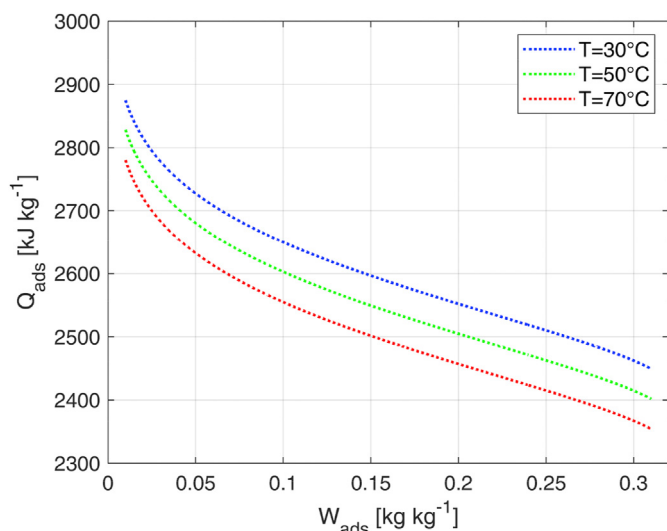


Fig. 4. Calculated heat of adsorption of silica gel (Eq. (22)).

3.3. Model validation

3.3.1. Experimental setup

As shown in Fig. 5, the test rig adopted in this research mainly consists of two beds filled with spherical silica gel beads, four 2-way commutation valves and plastic ducts. The two beds have cylindrical geometry ($D_{bed} = 25 \text{ cm}$, $H_{bed} = 40 \text{ cm}$) and are made of transparent plastic in order to allow the control of the correct desiccant beads disposal. During experimental tests, the two beds were adequately insulated to minimize heat losses through the surrounding. Packed beds inlet and outlet air states were measured with coupled temperature and humidity probes. More precisely, PT100 thermoresistances ($\pm 0.2 \text{ }^\circ\text{C}$ at $20 \text{ }^\circ\text{C}$) and relative humidity capacitive sensors ($\pm 1\%$ at $20 \text{ }^\circ\text{C}$) have been used. Airflow rates are evaluated through orifices plates and piezo-resistive pressure sensors ($\pm 0.5\%$ of reading $\pm 1 \text{ Pa}$), which have been installed according to international standards [30]. Each bed was alternatively crossed by the process and the regeneration airstream through the variation of the position of the four commutation valves. In both cases air flowed vertically, from the bottom to the top of the bed (co current arrangement). Finally, air conditions (temperature, humidity and flowrate) have been controlled through two independent air handling units equipped with heating coils, electric heaters, cooling coils, evaporative humidifiers and variable speed fans.

3.3.2. Comparison between numerical results and experimental data

Numerical results of the model have been compared with experimental data in two different operating conditions, as summarized in Table 2. Each experimental test has been repeated for several cycles, in order to get a time behaviour of outlet air conditions unaffected by the initial ones. In Figs. 6 and 7, humidity ratio and temperature profiles of the last three cycles are reported, respectively for Test 1 and Test 2. Combined instrumental uncertainty has been calculated according to standards [31]: depending on moist air state, uncertainty of X_a varies between 0.27 g kg^{-1} and 1.1 g kg^{-1} while uncertainty of T_a between $0.20 \text{ }^\circ\text{C}$ and $0.29 \text{ }^\circ\text{C}$. Instead, uncertainty of mass airflow rate is within $\pm 3\%$ of the calculated value.

Numerical simulations are carried out with a time step of 1 s and using as input the conditions of the air ($T_{a,in}$, $X_{a,in}$ and $v_{a,in}$) measured at the entrance of the bed.

In both tests, there is a good agreement between numerical and experimental data. In Test 1, relative differences between numerical and experimental data of $\Delta \bar{X}_a$ and $\Delta \bar{T}_a$ are equal to 2% and -30% in the regeneration period; 1% and 7% in the process period. Also in Test 2, model effectively reproduces measured data: in this case relative differences between numerical results and tests of $\Delta \bar{X}_a$ and $\Delta \bar{T}_a$ are equal to 7% and -12% in the regeneration period and -5% and -8% in the process period. The main deviation occurs in the outlet air temperature during the regeneration period, where numerical values are higher than measured ones. This effect is mainly related to heat losses to the surrounding of the experimental setup, which increase with the airflow temperature. In fact, in Test 2 average regeneration temperature is lower than one of Test 1 and, accordingly to the aforementioned considerations, also the difference of $\Delta \bar{T}_a$ between numerical and experimental data is significantly lower. Finally, considering that the present study focuses on humidification capacity of the proposed device, it is possible to state the model is an adequate tool to perform the analysis, being relative differences of $\Delta \bar{X}_a$ always within 7%.

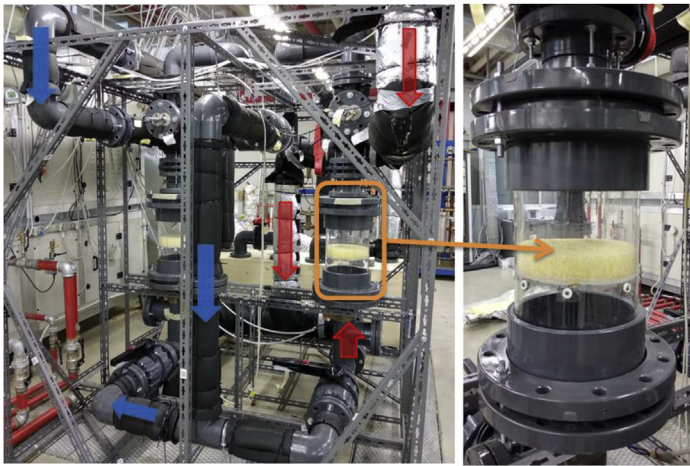


Fig. 5. View and scheme of the experimental setup.

Table 2
Conditions of tests used for model validation.

| | Test 1 | Test 2 |
|--|--------|--------|
| L_{bed} [cm] | 5.5 | 5.5 |
| τ ($=\tau_{pro} = \tau_{reg}$) [s] | 1800 | 1800 |
| v_{pro}^N [$m\ s^{-1}$] | 0.60 | 0.56 |
| v_{reg}^N [$m\ s^{-1}$] | 0.55 | 0.56 |
| $\bar{T}_{pro,in}$ [$^{\circ}C$] ¹ | 32.3 | 33.0 |
| $\bar{T}_{reg,in}$ [$^{\circ}C$] ¹ | 55.7 | 46.5 |
| $\bar{X}_{pro,in}$ [$g\ kg^{-1}$] ¹ | 7.9 | 16.0 |
| $\bar{X}_{reg,in}$ [$g\ kg^{-1}$] ¹ | 7.1 | 10.8 |

Note: ¹ Averaged quantity calculated in the last cycle.

4. Numerical analysis of the system

4.1. Preliminary considerations

In this section, a numerical analysis of the proposed humidification system is carried out, in order to evaluate main effects of suitable configurations and different operating conditions on performance. According to Fig. 1, reference configuration and operating conditions are set in the following way:

- 1) Airflows are in co-current arrangement, the bed thickness L_{bed} is set equal to 5.5 cm and desiccant beads diameter D_b is equal to 3.3 mm, similarly to the arrangement adopted in the experimental tests.
- 2) Inlet process airflow state pro,in is assumed at typical indoor winter air conditions, namely $T_{pro,in} = 20\ ^{\circ}C$ and $X_{pro,in} = 5.8\ g\ kg^{-1}$ ($RH_{pro,in} = 40\%$).
- 3) Inlet humidity ratio of regeneration air stream $X_{reg,in}$ is equal to one of outdoor air, assumed at $1.5\ g\ kg^{-1}$. This value represents a peak condition (minimum value) of winter climate in Northern Italy (Milan).
- 4) The air velocity v_a^N is set at $0.5\ m\ s^{-1}$ for both air flows, in order to have a pressure drop through the bed around 150 Pa. This value, which has been evaluated through the Ergun equation [32], represents typical pressure drop of heat exchangers in AHUs.

The regeneration temperature $T_{reg,in}$ and the commutation period τ (half cycle, being $\tau = \tau_{pro} = \tau_{reg}$) are independently set, in order to find the optimal operating conditions. Inlet airflow

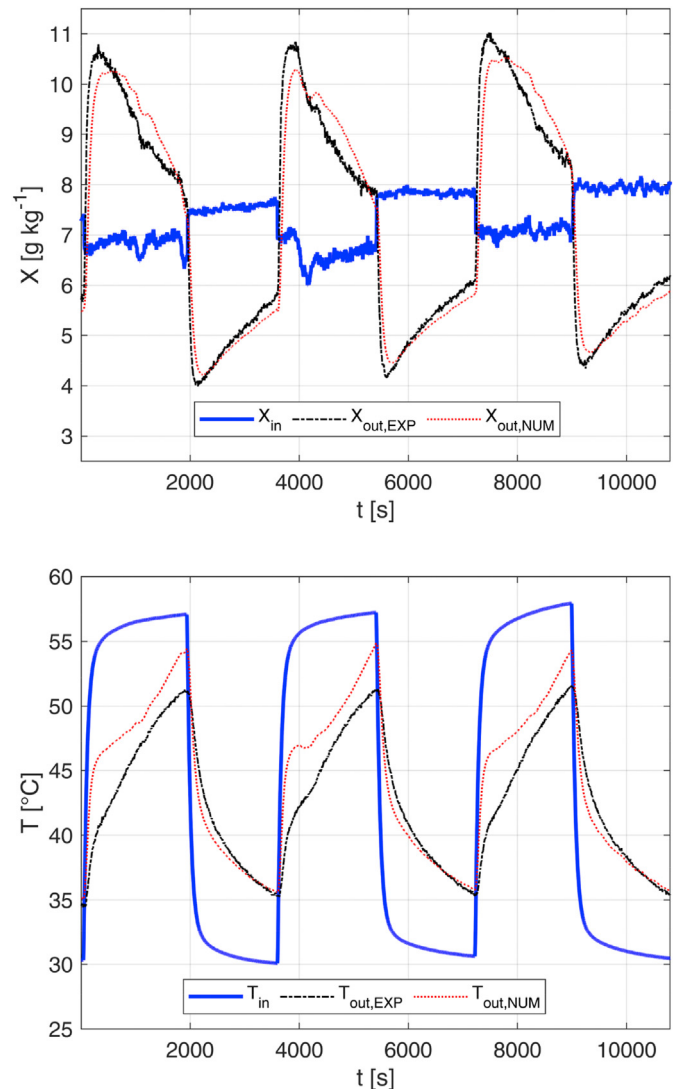


Fig. 6. Test 1 - Comparison between experimental data and numerical results: humidity ratio and temperature ($\tau = 1800\ s$; $v_{pro}^N = 0.60\ m\ s^{-1}$; $v_{reg}^N = 0.55\ m\ s^{-1}$; $L_{bed} = 5.5\ cm$).

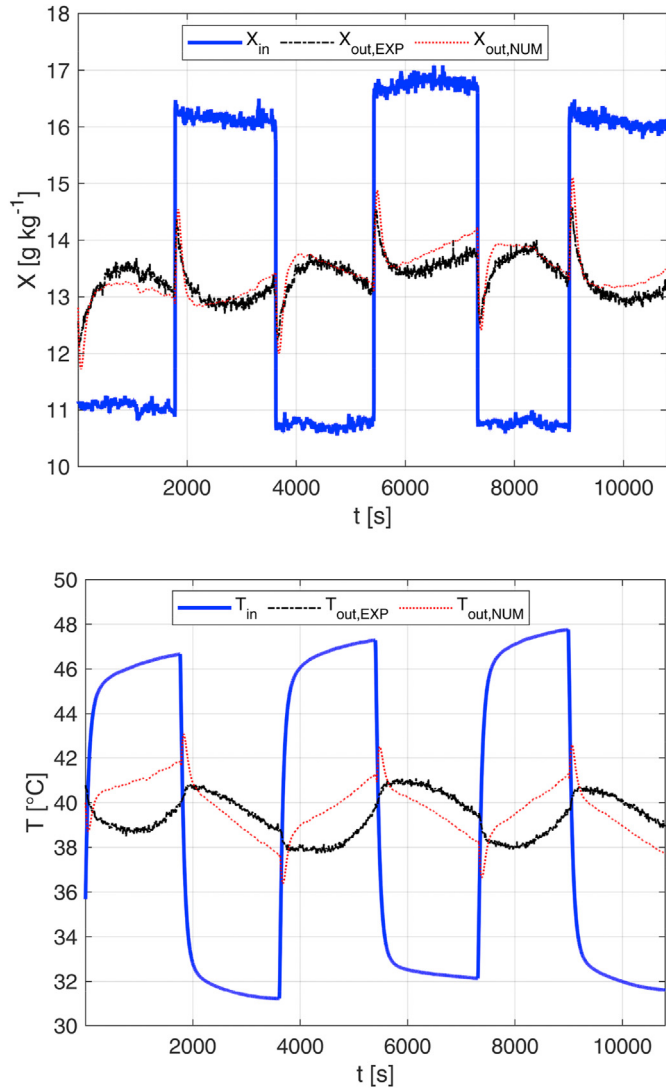


Fig. 7. Test 2 - Comparison between experimental data and numerical results: humidity ratio and temperature ($\tau = 1800$ s; $v_{pro}^N = 0.56$ m s⁻¹; $v_{reg}^N = 0.56$ m s⁻¹; $L_{bed} = 5.5$ cm).

conditions are assumed constant respectively during the process and regeneration period ($X_{a,in} = \bar{X}_{a,in}$ and $T_{a,in} = \bar{T}_{a,in}$). $T_{reg,in}$ is varied in the range between 20 °C and 60 °C, in order to evaluate the combination with low temperature heat sources. Particular attention is given to the analysis of the regeneration airflow, whose outlet conditions represent the useful effect of the humidification system.

4.2. Effect of regeneration temperature and commutation time

Effect of $T_{reg,in}$ and τ variation is investigated and results are shown in Fig. 8. Similarly to recent researches about performance of desiccant wheels [33–36], the higher the regeneration temperature, the higher $\bar{X}_{reg,out}$. The trend is related to the decrease of $RH_{reg,in}$, which leads to a lower W_{ads} at equilibrium condition and, in turn, to a higher release of water to the air stream during the regeneration process. Moreover, the commutation time influences the outlet air conditions: if the regeneration period is too long, desiccant beads reach their minimum water content and they are not able to humidify the airflow anymore. On the other side, if the

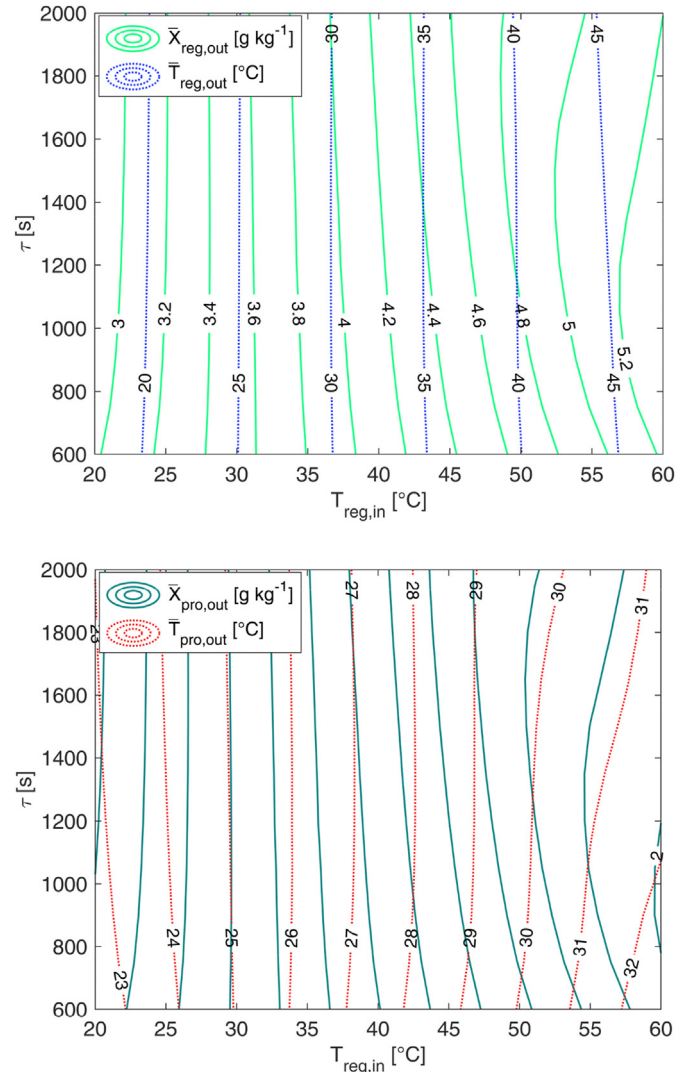


Fig. 8. Average outlet temperature and humidity ratio of regeneration and process airflows in the reference configuration ($v_{pro}^N = v_{reg}^N = 0.5$ m s⁻¹; $L_{bed} = 5.5$ cm; $X_{reg,in} = 1.5$ g kg⁻¹; $T_{pro,in} = 20$ °C; $X_{pro,in} = 5.8$ g kg⁻¹; co-current flows).

regeneration period is too short, the commutation occurs when the desiccant material is still able to desorb water. Consequently, an optimal commutation time exists: in the investigated conditions, it is between 1200 s and 1500 s, with a limited variation in the range. The outlet regeneration temperature is mainly influenced by the inlet one, with slight variation due to change in the commutation time. The maximum $\bar{X}_{reg,out}$ is 5.3 g kg⁻¹, obtained at $T_{reg,in} = 60$ °C and $\tau = 1200$ s. It is put in evidence that in this condition $\bar{T}_{reg,out}$ is around 48 °C: it is a high value that could cause discomfort to building occupants. For this reason, a heat recovery device could be necessary to reduce $\bar{T}_{reg,out}$ before the airflow is supplied to the indoor environment. Similar conclusions can be drawn by analysing process airflow outlet conditions. Finally, it is highlighted that in this operating condition a satisfactorily airflow humidification ($\bar{X}_{reg,out}$ around 4.5 g kg⁻¹) is obtained also when $T_{reg,in}$ approaches 45 °C.

4.3. Effect of bed length

In Fig. 9, the effect of bed length for two different commutation

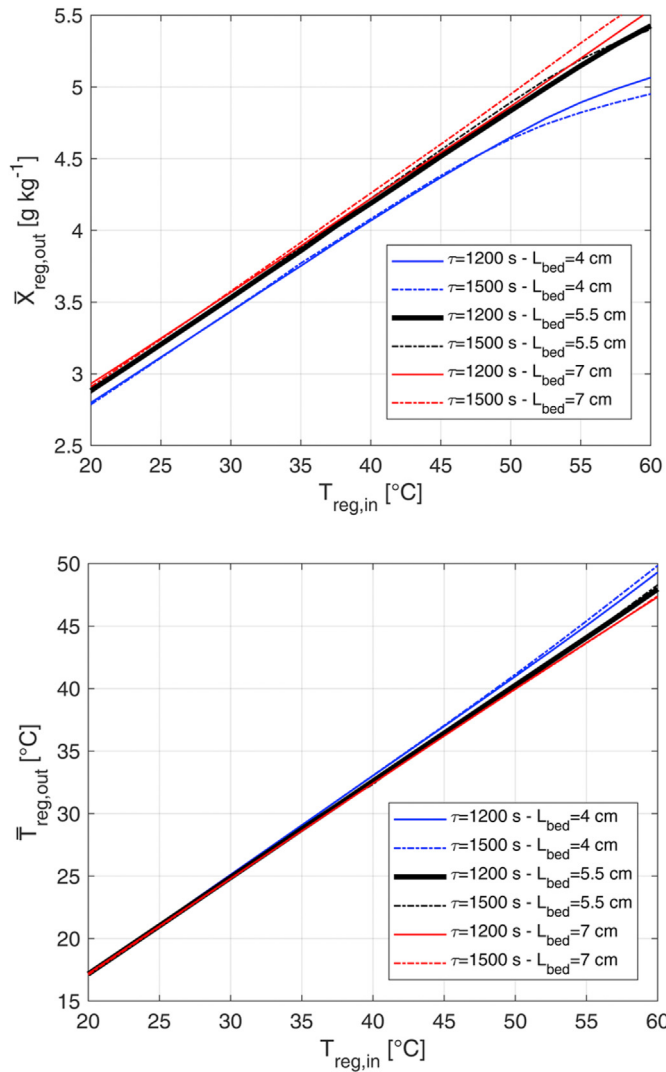


Fig. 9. Effect of cycle time and bed length on average outlet temperature and humidity ratio of regeneration airflow ($v_{pro}^N = v_{reg}^N = 0.5 \text{ m s}^{-1}$; $X_{reg,in} = 1.5 \text{ g kg}^{-1}$; $T_{pro,in} = 20 \text{ }^\circ\text{C}$; $X_{pro,in} = 5.8 \text{ g kg}^{-1}$; co-current flows).

periods is investigated: L_{bed} is reduced and increased by 1.5 cm compared to the reference condition (with $L_{bed} = 5.5 \text{ cm}$) and τ is set to 1200 s and 1500 s (values within the optimal range discussed in Section 5.2). An increase in L_{bed} leads to an increase in $\bar{X}_{reg,out}$ due to the higher quantity of desiccant material in the bed. Anyway, in this case the optimal commutation time can be slightly different from the one evaluated for the reference case. In fact, the higher the mass of silica gel, the higher the time required to adsorb and desorb water vapour. Finally, $\bar{T}_{reg,out}$ is mainly influenced by $T_{reg,in}$ without significant variations among the investigated cases.

4.4. Effect of air velocity

In Fig. 10, the effect of inlet airflow velocity is shown for two different commutation periods. Numerical results highlight that an increase in the velocity of both airflows leads to a slight reduction of the humidification capacity. In fact, in these operating conditions, the effect of the lower air residence time in the bed is partially compensated by the higher heat and mass transfer rate (related to the increase of h_c and h_m). At the same time, the desiccant bed tends to release the adsorbed water in a shorter time and, for this reason,

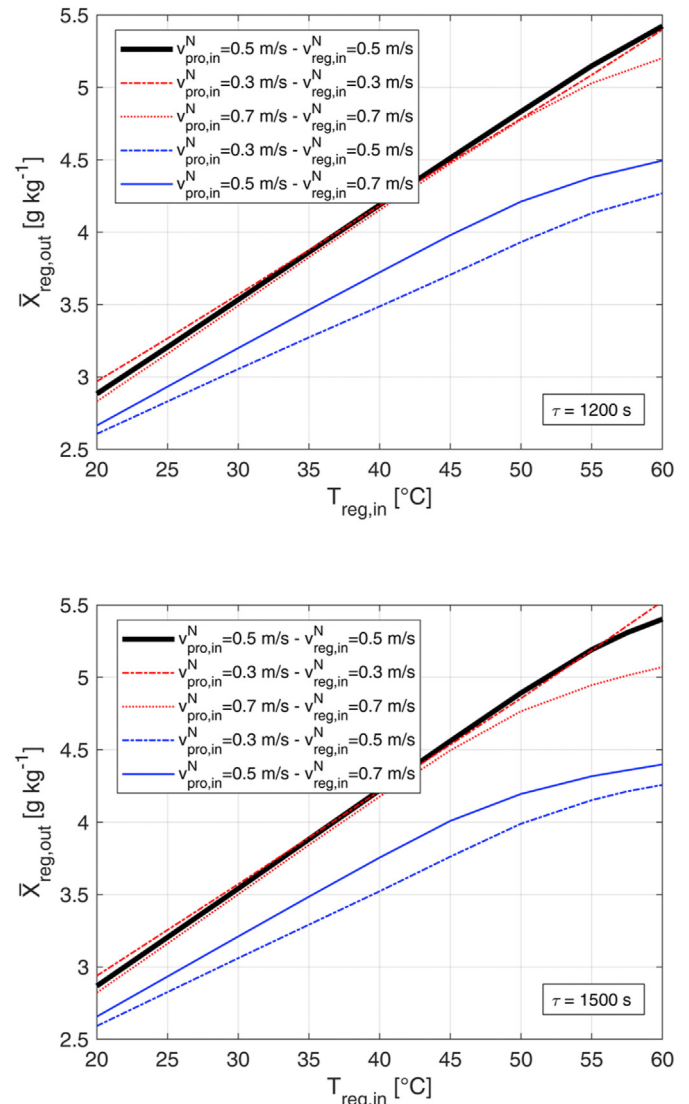


Fig. 10. Effect of inlet velocities on average outlet humidity ratio of regeneration airflow ($L_{bed} = 5.5 \text{ cm}$; $X_{reg,in} = 1.5 \text{ g kg}^{-1}$; $T_{pro,in} = 20 \text{ }^\circ\text{C}$; $X_{pro,in} = 5.8 \text{ g kg}^{-1}$; co-current flows).

a reduction of the commutation time is suggested. Similar considerations can be drawn in case of reduction of the airflow rates.

In addition, two cases with unbalanced airflows have been investigated: in both cases, the process air stream (return from the building) has been assumed lower than the regeneration one (fresh air supplied to indoor environment), according to actual applications. The humidification capacity of the system decreases because, during the process period, a lower amount of water is adsorbed from the desiccant material. In addition, the higher the regeneration to process mass flow ratio, the lower the humidification capacity. This effect should be properly taken into account in the design of the system, in order to avoid underestimation of the performance of the humidifier.

4.5. Effect of air inlet conditions

In this section, the effect of different inlet air conditions is discussed by varying one by one: $T_{pro,in}$, $X_{pro,in}$ and $X_{reg,in}$. According to results shown in Fig. 11, the following considerations can be made:

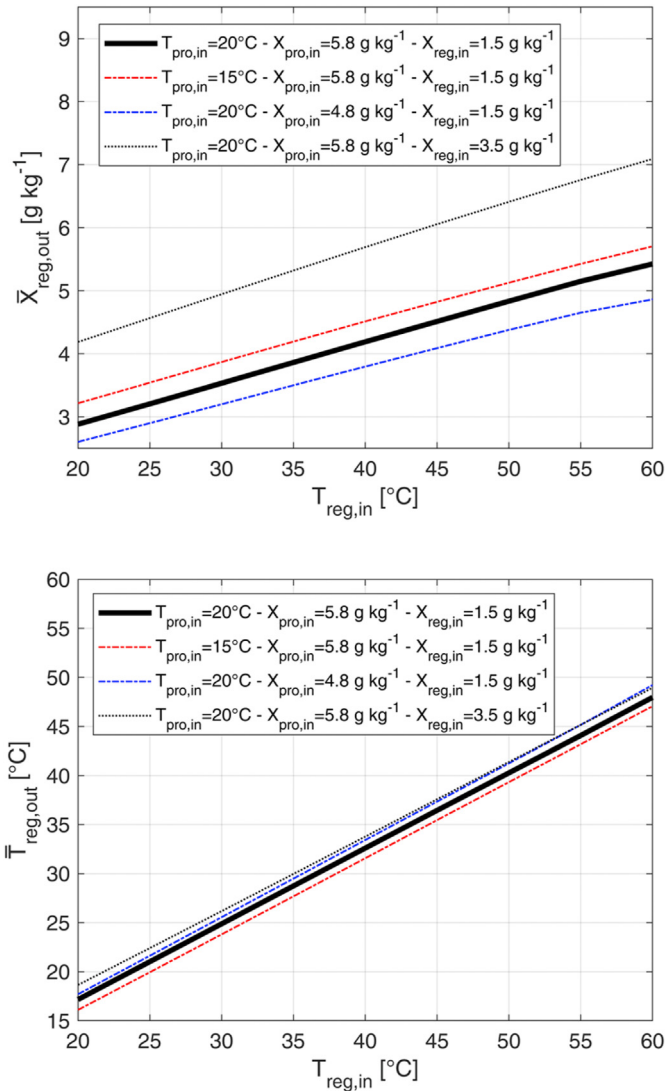


Fig. 11. Effect of inlet air conditions on average outlet temperature and humidity ratio of regeneration airflow ($\tau = 1200$ s; $L_{bed} = 5.5$ cm; $v_{pro}^N = v_{reg}^N = 0.5$ m s⁻¹; co-current flows).

- A decrease in $T_{pro,in}$ leads to an increase in $RH_{pro,in}$ and, therefore, in the quantity of vapour adsorbed during the process period. The same amount of vapour is released during the regeneration period and, consequently, the humidification capacity increases. For this reason, the use of a heat exchanger to cool down the return air from the building is a suitable option to be adopted in order to increase system performance.
- A reduction in $X_{pro,in}$ leads to a decrease in $RH_{pro,in}$; similarly to explanation provided for the previous case, in this situation $\bar{X}_{reg,out}$ reduces. In addition, $X_{pro,in}$ is a limiting factor: since $\bar{X}_{pro,out}$ can at most approach 0 g kg⁻¹, a reduction in the initial water content lead to a reduction of the maximum quantity of adsorbed water and, consequently, of the system humidification capacity.
- Finally, it is shown that the higher $X_{reg,in}$, the higher $\bar{X}_{reg,out}$. Anyway, it is put in evidence that $\Delta\bar{X}_{reg}$ slightly decreases compared to the reference case because, at constant $T_{reg,in}$, there is an increase in $RH_{reg,in}$ with consequent limiting effect on the desiccant regeneration process.

In all simulations, as already discussed, the trend of the outlet regeneration temperature is mainly related to $T_{reg,in}$.

4.6. Effect of counter flow arrangement

The effect of counter-current arrangement is investigated in Fig. 12 for two different bed lengths. In the first case it is set equal to the reference condition ($L_{bed} = 5.5$ cm): humidification capacity, quite obviously, increases and $\bar{X}_{reg,out}$ reaches a maximum value of 5.9 g kg⁻¹ when τ is 600 s and $T_{reg,in} = 60$ °C. It is highlighted that the optimal commutation time that maximizes the system performance, compared to the co-current configuration, slightly decreases. This effect can be explained considering that in this flow arrangement heat and mass transfer are more effective and, therefore, the system approaches the equilibrium condition in a shorter time. Instead, if the bed length is set to 7 cm, the maximum $\bar{X}_{reg,out}$ is even around 6.1 g kg⁻¹. Therefore, the analysis puts in evidence that the proposed system, when L_{bed} is around 5.5–7 cm, can transfer a significant amount of water vapour from the return

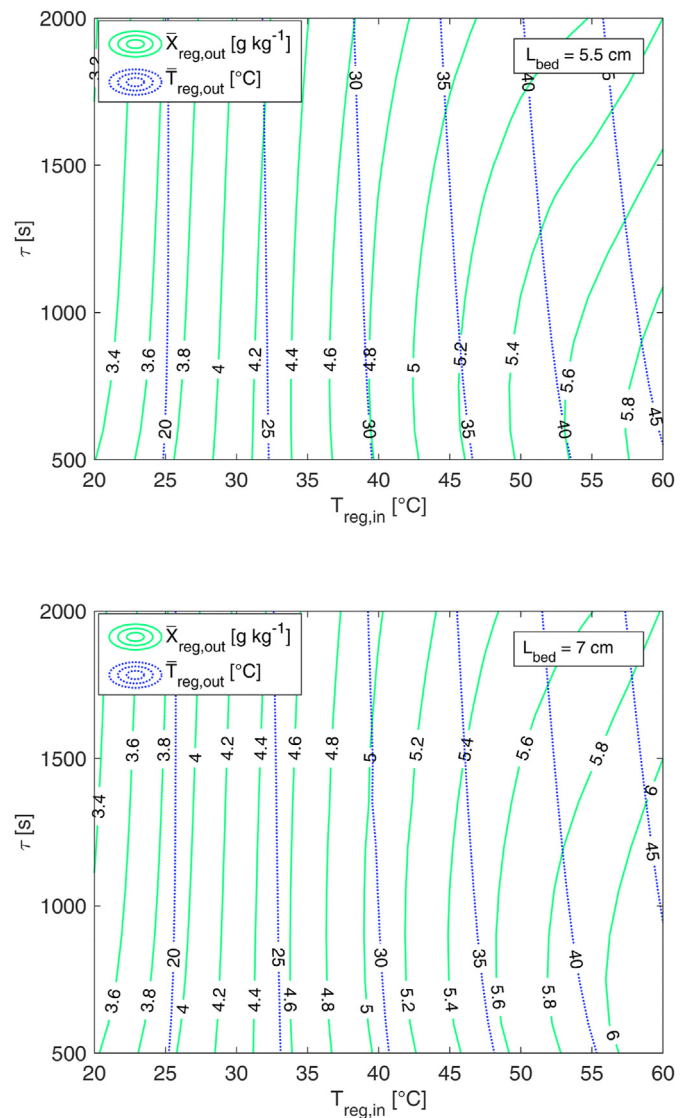


Fig. 12. Average outlet temperature and humidity ratio of regeneration airflow in counter-current configuration ($v_{pro}^N = v_{reg}^N = 0.5$ m s⁻¹; $X_{reg,in} = 1.5$ g kg⁻¹; $T_{pro,in} = 20$ °C; $X_{pro,in} = 5.8$ g kg⁻¹; counter-current flows).

airflow (process stream) to the one supplied to the building (regeneration stream). In particular, when $\bar{X}_{reg,out} = X_{pro,in} = 5.8 \text{ g kg}^{-1}$ (obtained at $T_{reg,in}$ equal to $57 \text{ }^\circ\text{C}$ or $52 \text{ }^\circ\text{C}$), the humidification system is able to keep a constant humidity ratio in the built environment even without any indoor latent load. Instead, if there are latent loads inside the building, as it typically occurs in presence of people, the system can effectively maintain the desired humidity level supplying air at $\bar{X}_{reg,out} < 5.8 \text{ g kg}^{-1}$ with a regeneration temperature below $50 \text{ }^\circ\text{C}$. Finally, it is highlighted that the analysis is carried out assuming humidity ratio of outdoor air at 1.5 g kg^{-1} . This value is quite low and represents peak winter conditions: in moderate climates, when the outdoor humidity ratio is around $3\text{--}3.5 \text{ g kg}^{-1}$, the system can easily increase the water content of the airflow supplied to the building up to the desired condition.

4.7. Comparison with conventional humidification technologies

In this section, power consumption of the proposed humidification system (counter-current flows, $L_{bed} = 5.5 \text{ cm}$, $\tau = 1000 \text{ s}$, $v^N = 0.5 \text{ m s}^{-1}$) is compared to ones of adiabatic and steam humidifiers in different representative operating conditions. Referring to the psychrometric chart of Fig. 13, the heating process $e-1$ is common to all technologies and it is necessary to increase the saturation pressure of water, in order to allow the subsequent air humidification. On the other hand, the isobaric humidification occurring between state 1 and state out differs for the three systems as follows:

- Desiccant Humidifier (DH): heating at constant humidity ratio (from 1 to $1''$) and, then, desorption of water from the desiccant bed (from $1''$ to out).
- Adiabatic Humidifier (AH): heating at constant humidity ratio (from 1 to $1'$) and, then, evaporation of liquid water in the airflow (from $1'$ to out). This second process can be roughly considered at constant moist air specific enthalpy.

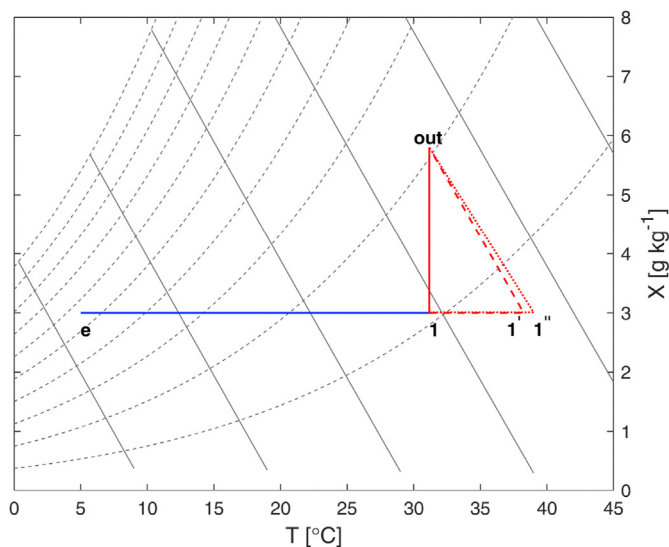


Fig. 13. Qualitative representation of humidification process on the psychrometric chart ($p_{tot} = 101325 \text{ Pa}$): i) pre heating (blue solid line); ii) steam humidifier (red solid line); iii) adiabatic humidifier (red dashed line); iv) desiccant humidifier (red dotted line). (For interpretation of the references to colour in this figure legend, the reader is referred to the Web version of this article.)

- Steam Humidifier (SH): supply of steam, generated in a dedicated equipment, to the air stream (from 1 to out). The process is approximately at constant dry bulb temperature.

Three different winter operating conditions are investigated (weather of Milan), as shown in Table 3. The first case (reported in Fig. 13) refers to a typical day with medium-low outdoor air humidity ratio and the second one to a day with medium-high values. The last case is equal to the first one with a lower inlet process air temperature, representing the configuration with a sensible heat recovery system between fresh and exhaust airflows. For each case, the inlet regeneration temperature of the desiccant humidifier, providing the desired outlet humidity ratio ($\bar{X}_{reg,out} = X_{out}$), is set and the corresponding outlet regeneration temperature is evaluated. The initial humidification temperature T_1 is set equal to $\bar{T}_{reg,out}$: in this way, all the transformations occurring in the three systems between state 1 and state out can be compared.

Specific energy consumption (referred to the mass of air) of each humidifier is calculated as:

$$\dot{q}_{DH} = c_p (T_1'' - T_1) \quad (23)$$

$$\dot{q}_{AH} = c_p (T_1' - T_1) \quad (24)$$

$$\dot{q}_{SH} = h_v (X_{out} - X_1) \quad (25)$$

Finally, in order to properly compare the investigated technologies on a common basis, specific power consumption referred to the primary energy source is calculated. In particular, desiccant and adiabatic humidifiers are supposed to be driven by a low temperature heat source ($\eta_{th,lt} = 0.9$) while the steam humidifier by a high temperature heat source ($\eta_{th,ht} = 0.8$) or by electricity ($\eta_{el} = 0.5$). Therefore, it results:

$$\dot{q}_{p,DH} = \frac{\dot{q}_{DH}}{\eta_{th,lt}} \quad (26)$$

$$\dot{q}_{p,AH} = \frac{\dot{q}_{AH}}{\eta_{th,lt}} \quad (27)$$

$$\dot{q}_{p,SH,th} = \frac{\dot{q}_{SH}}{\eta_{th,ht}} \quad (28)$$

$$\dot{q}_{p,SH,el} = \frac{\dot{q}_{SH}}{\eta_{el}} \quad (29)$$

According to results of Table 4, it is possible to state:

- Specific energy consumption q of SH and AH is slightly lower than the one of DH (from -7.3% to -9.6%). In fact, the extra energy provided to the air stream in process $1'-1''$ is necessary because the heat of adsorption is higher than the enthalpy of

Table 3
Conditions of analysed cases.

| Case | 1 | 2 | 3 |
|--|------|------|------|
| $X_{pro,in} [\text{g kg}^{-1}]$ | 5.8 | 5.8 | 5.8 |
| $T_{pro,in} [^\circ\text{C}]$ | 20.0 | 20.0 | 10.0 |
| $X_e = X_{reg,in} [\text{g kg}^{-1}]$ | 3.0 | 4.5 | 3.0 |
| $X_{out} = \bar{X}_{reg,out} [\text{g kg}^{-1}]$ | 5.8 | 5.8 | 5.8 |
| $T_{reg,in} [^\circ\text{C}]$ | 39.0 | 28.0 | 28.1 |
| $T_1 = \bar{T}_{reg,out} [^\circ\text{C}]$ | 31.2 | 24.5 | 20.4 |

Table 4
Specific energy consumption of different humidifiers.

| Case | 1 | 2 | 3 |
|--|------|-----|------|
| \dot{q}_{DH} [kJ kg ⁻¹] | 7.9 | 3.6 | 7.7 |
| \dot{q}_{AH} [kJ kg ⁻¹] | 7.1 | 3.3 | 7.1 |
| \dot{q}_{SH} [kJ kg ⁻¹] | 7.1 | 3.3 | 7.1 |
| $\dot{q}_{p,DH}$ [kJ kg ⁻¹] | 8.8 | 4.0 | 8.6 |
| $\dot{q}_{p,AH}$ [kJ kg ⁻¹] | 7.9 | 3.7 | 7.9 |
| $\dot{q}_{p,SH,th}$ [kJ kg ⁻¹] | 8.9 | 4.1 | 8.9 |
| $\dot{q}_{p,SH,el}$ [kJ kg ⁻¹] | 14.3 | 6.6 | 14.2 |

water evaporation and because both the air and the desiccant material need heating.

- Specific primary energy consumption $q_{p,SH,th}$ of high temperature driven SH is slightly higher than the one of DH (between +1.7% and +4.2%). Anyway, it should be highlighted that the steam humidifier requires a high temperature heat source (>100 °C) and that it cannot be driven by waste heat or typical renewable energy sources.
- Quite obviously, specific primary energy consumption of electric steam humidifier is around 65% higher than desiccant based technology, due to the low conversion efficiency.
- It is well known that specific energy consumption of conventional AH is slightly lower than the one of DH but the two technologies are not directly comparable due to the risk of bacterial proliferation related to the presence of liquid water, as discussed in Section 1.

Finally, it is worth specifying that pressure losses are not considered in the comparison because they depend specifically on system configuration. In any case, it should be noted that the humidification system based on desiccant beads has a pressure loss slightly higher than the others, due to the presence of two silica gel beds.

5. Conclusions

In this research a packed bed desiccant humidification system is analysed through an experimental a numerical approach. Preliminary results of this study put in evidence that:

- The lumped parameter model proposed by Pesaran and Mills [24], appropriately integrated with properties of the silica gel adopted in the test rig, can effectively reproduce experimental data.
- A bed length around 5.5–7 cm can provide adequate humidification of the fresh airflow supplied to the building, when face velocity is around 0.5 m s⁻¹.
- When return air from the building is at 20 °C and at 5.8 g kg⁻¹, the humidity ratio of the airflow supplied to the building can be increased from 1.5 g kg⁻¹ to 5.3–6.1 g kg⁻¹ with a regeneration temperature around 60 °C, depending on flow configuration and bed length. Meanwhile, the outlet air temperature is in the range 43–48 °C.
- In typical average winter conditions, the system can provide adequate air humidification with inlet regeneration temperature below 50 °C, highlighting that it can be coupled with solar thermal collectors, cogenerators or it can be driven by industrial waste heat or district heating.
- The system can be driven by low temperature heat sources compared to conventional steam humidifiers.

- Performance of counter-current flow arrangement is higher than one of co-current configuration.

Based on aforementioned promising results, further studies should deal with the design and optimization of the system and its integration in air handling units.

Authors' individual contributions

Stefano De Antonellis, Supervision, Conceptualization, Data curation, Formal analysis, Investigation, Methodology, Validation, Writing - original draft, Writing - review & editing. Luigi Colombo, Conceptualization, Data curation, Investigation, Methodology, Writing - original draft, Writing - review & editing. Angelo Freni, Conceptualization, Investigation, Methodology, Writing - original draft, Writing - review & editing. Cesare Joppolo, Conceptualization, Writing - original draft, Writing - review & editing.

Declaration of competing interest

The authors declare that they have no known competing financial interests or personal relationships that could have appeared to influence the work reported in this paper.

Acknowledgments

Funding for this work from FARB (2016) and interdepartmental laboratory CECH (2015) - Politecnico di Milano - is acknowledged.

References

- [1] Wolkoff P. Indoor air humidity, air quality, and health—An overview. *Int J Hyg Environ Health* 2018;221(3):376–90.
- [2] Derby MM, Hamehkasi M, Eckels S, Hwang GM, Jones B, Maghirang R, Shulan D. Update of the scientific evidence for specifying lower limit relative humidity levels for comfort, health, and indoor environmental quality in occupied spaces (RP-1630). *Science and Technology for the Built Environment* 2017;23(1):30–45.
- [3] Xie X, Li Y, Chwang AT, Ho PL, Seto WH. How far droplets can move in indoor environments—revisiting the Wells evaporation-falling curve. *Indoor Air* 2007;17(3):211–25.
- [4] ASHRAE Handbook. HVAC systems and equipment. Atlanta, USA: American Society of Heating, Refrigerating and Air-conditioning Engineers; 2013.
- [5] Kovak B, Heimann PR, Hammel J. The sanitizing effects of desiccant-based cooling. *ASHRAE J* 1997;39(4):60.
- [6] Straus D, Larranaga MD, Karunasena E, Holder HW, Beruvides MG. Improving the quality of the indoor environment utilizing desiccant-assisted heating, ventilating, and air conditioning systems. In: Chemistry, emission control, radioactive pollution and indoor air quality. IntechOpen; 2011.
- [7] De Antonellis S, Intini M, Joppolo CM, Pedranzini F. Experimental analysis and practical effectiveness correlations of enthalpy wheels. *Energy Build* 2014;84:316–23.
- [8] Fu H, Liu X, Xie Y, Jiang Y. Experimental and numerical analysis on total heat recovery performance of an enthalpy wheel under high temperature high humidity working conditions. *Appl Therm Eng* 2019;146:482–94.
- [9] Niemann P, Schmitz G. Experimental investigation of a ground-coupled air conditioning system with desiccant assisted enthalpy recovery during winter mode. *Appl Therm Eng* 2019;160:114017.
- [10] La D, Dai Y, Li H, Li Y, Kiplagat JK, Wang R. Experimental investigation and theoretical analysis of solar heating and humidification system with desiccant rotor. *Energy Build* 2011;43(5):1113–22.
- [11] Zeng DQ, Li H, Dai YJ, Xie AX. Numerical analysis and optimization of a solar hybrid one-rotor two-stage desiccant cooling and heating system. *Appl Therm Eng* 2014;73(1):474–83.
- [12] Kawamoto K, Cho W, Kohno H, Koganei M, Ooka R, Kato S. Field study on humidification performance of a desiccant air-conditioning system combined with a heat pump. *Energies* 2016;9(2):89.
- [13] De Antonellis S, Intini M, Joppolo CM, Molinaroli L, Romano F. Desiccant wheels for air humidification: an experimental and numerical analysis. *Energy Convers Manag* 2015;106:355–64.
- [14] Cazzaniga E, Colombo L, De Antonellis S. Preliminary experimental and numerical analysis of a silica gel packed bed humidification system. 13th REHVA world congress, CLIMA, vol. 111. EDP Sciences; 2019. p. 1–6.
- [15] Tu R, Li J, Hwang Y. Fresh air humidification in winter using desiccant wheels for cold and dry climate regions: optimization study of humidification

- processes. *Int J Refrig* 2020;118:121–30.
- [16] Kawazoe M., Matsui N., Yonemoto K., US2006/260332A1, Humidity controller apparatus, US Patent Office.
- [17] Egaitsu T., Fukuchi T., Ikemoto H., Tsujimoto S. JP2003074906A, Desiccant dehumidification apparatus, Japanese Patent Office.
- [18] De Antonellis S. 10202000000439 (pending patent), *Sistema di umidificazione d'aria*, Italian Patent Office.
- [19] Sun XY, Dai YJ, Ge TS, Zhao Y, Wang RZ. Investigation on humidification effect of desiccant coated heat exchanger for improving indoor humidity environment in winter. *Energy Build* 2018;165:1–14.
- [20] Ge TS, Dai YJ, Wang RZ. Performance study of desiccant coated heat exchanger air conditioning system in winter. *Energy Convers Manag* 2016;123:559–68.
- [21] Zhang JY, Ge TS, Dai YJ, Zhao Y, Wang RZ. Experimental investigation on solar powered desiccant coated heat exchanger humidification air conditioning system in winter. *Energy* 2017;137:468–78.
- [22] Valarezo AS, Sun XY, Ge TS, Dai YJ, Wang RZ. Experimental investigation on performance of a novel composite desiccant coated heat exchanger in summer and winter seasons. *Energy* 2019;166:506–18.
- [23] Valarezo AS, Sun XY, Ge TS, Dai YJ, Wang RZ. Experimental investigation on performance of a novel composite desiccant coated heat exchanger in summer and winter seasons. *Energy* 2019;166:506–18 (last access the 18th of March 2020), <https://polybloc.com/en/products/accubloc/>.
- [24] Pesaran AA, Mills AF. Moisture transport in silica gel particle beds: I. Theoretical study (No. NREL/TP-252-2388). Golden, CO (United States): National Renewable Energy Lab.(NREL); 1986.
- [25] John C. Slattery, advanced transport phenomena. Ch. 4, 7 and 10. Cambridge University Press; 1999.
- [26] Ruthven DM. Principles of adsorption and adsorption processes. John Wiley & Sons; 1984.
- [27] Goldsworthy MJ. Measurements of water vapour sorption isotherms for RD silica gel, AQSOA-Z01, AQSOA-Z02, AQSOA-Z05 and CECA zeolite 3A. *Microporous Mesoporous Mater* 2014;196:59–67.
- [28] Aristov YI, Tokarev MM, Freni A, Glaznev IS, Restuccia G. Kinetics of water adsorption on silica Fuji Davison RD. *Microporous Mesoporous Mater* 2006;96(1–3):65–71.
- [29] Frazzica A, Cabeza LF, editors. Recent advancements in materials and systems for thermal energy storage: an introduction to experimental characterization methods. Springer; 2018.
- [30] DIN EN ISO 5167-2 Standards, Measurement of fluid flow by means of pressure differential devices inserted in circular cross-section conduits running full—Part 2: Orifice plates (ISO 5167-2:2003).
- [31] Frazzica A, Cabeza LF, editors. ISO IEC guide 98-3, uncertainty of measurement—Part 3: guide to expression of uncertainty in measurement. Geneva Switzerland: International Organization for Standardization; 2008. ISO IEC Guide 98-3.
- [32] Ergun S. Fluid flow through packed columns. *Chem Eng Prog* 1952;48:89–94.
- [33] De Antonellis S, Joppolo CM, Molinaroli L. Simulation, performance analysis and optimization of desiccant wheels. *Energy Build* 2010;42(9):1386–93.
- [34] De Antonellis S, Intini M, Joppolo CM. Desiccant wheels effectiveness parameters: correlations based on experimental data. *Energy Build* 2015;103:296–306.
- [35] De Antonellis S, Intini M, Joppolo CM, Romano F. On the control of desiccant wheels in low temperature drying processes. *Int J Refrig* 2016;70:171–82.
- [36] Angrisani G, Minichiello F, Roselli C, Sasso M. Desiccant HVAC system driven by a micro-CHP: experimental analysis. *Energy Build* 2010;42(11):2028–35.